JCAMECH

Vol. 50, No. 1, June 2019, pp 99-107
DOI: 10.22059/jcamech.2019.276035.362

Micro-cantilevered MEMS Biosensor for detection of Malaria Protozoan Parasites

Kurmendra [a,], Jagdeep Rahul[a] and Rajesh Kumar[b]*

[a] *Department of Electronics & Communication Engineering, Rajiv Gandhi University (A Central University), Itanagar, India*
[b] *Department of Electronics & Communication Engineering, NERIST, Nirjuli, India*

ARTICLE INFO

Article history:
Received: 14 January 2019
Accepted: 22 February 2019

Keywords:
Biosensors
Malaria
MEMS
Microcantilever
Sensitivity

ABSTRACT

In this paper, the presented work aims to provide a designed model based on Finite element method for detection of Malaria protozoan parasites. Micro-cantilevers are next generation highly efficient biosensors for detection and prevention of any disease. Here, an E-shaped model for micro cantilevered biosensor is designed using COMSOL Multiphysics specifically for detection of Malaria. Microcantilever materials viz Au, Cu, Si and Pt are used for sensing Malaria protozoan with proper optimization of device structure. The studies were carried out for stress developed and displacement occurred due to force applied through these protozoan biomolecules and varying beam length. Further, the designed structure was analyzed for different beam materials available for biosensor and it was found that Au is best suitable material for detection of malaria protozoan parasites since it has best sensitivity profile among presented materials. The results were also verified through analytical approach and it was found that both results obtained through simulation and analytical methods do closely agree with each other.

1. Introduction

The MEMS technology has brought out a revolutionary change in the era of modern science and technology. It has found its application in medical, Bio-logical and communication engineering [1]. MEMS technology has opened new possibilities because of its eminent characteristics which results in miniaturization of device, low weight, and most impoortantly comsumes very less power. MEMS devices are seen to have much superior performances and smart functionalities. The MEMS technology is developing exponentially day-by-day and new products with wide range of applications are making the lives of common people better and easy going. Recently, it has found its application in the field of pathological test also. The whole medical community is looking forward to this technology that in the near future it will immensely change the diagnosis procedure of various diseases in a whole new way for emergency situations using biosensors based on MEMS technology.

A Bio-sensor is an analytical device that measures biological or chemical change by producing signals which is directly proportional to the concentration of the analyte. Bio-sensors are employed in applications such as disease monitoring, drug delivery, detection of pollutants, disease-causing micro-organisms and Bio-markers that are indicators of a disease [2]. After thorough study it is seen that MEMS had a wide range of applications and most prominently it is going to be a powerful tool in medical diagnosis in the near future. Any medical diagnosis for accurate confirmation, chemical analysis is the only solution till date but there arise certain situations that there is not enough time for a proper chemical analysis which may require certain amount of time and therefore for adding a confirmation level to the predictions of a certain disease in emergency situations by observing the symptoms, this research highly motivated to design a bio-sensor which can serve that purpose in some emergency situations to detect the presence of malaria parasite in human blood.

Malaria is a common infectious disease caused by mosquito bites that spreads through protozoan parasites. According to the WHO World Malaria Report 2016, Malaria mainly spreads and are deadly in the tropical and sub-tropical regions of America, Asia and Africa continents. Every year about 51.5 million people are infected by it and about 10 to 30 million people even die. Most of the victims are small children of sub-Saharan Africa [3]. The protozoan that causes malaria was named as Plasmodium by the Italian scientists Etteré Marchiafava and Angelo Cele. It is of four types and the most dangerous of which is the Falciparum and Plasmodium Vivax. The other two are the Plasmodium oval and Plasmodium malaria. This entire group is called 'Malaria Parasite'. Female anopheles' mosquitoes are the carrier of this parasite. The malaria parasite multiplies itself when they enter the human blood,

* Corresponding author. Tel.: +91- 8415912663; e-mail: kurmendra.nits@gmail.com

resulting in symptoms of anemia (dizziness, breathlessness, etc.). Apart from this, periodic fever, colds, and grief are also seen. In severe cases, the patient can go unconscious and may even die in acute cases. Several measures can be taken to prevent the spreading of malaria. Mosquito nets must be used while sleeping, empty open containers must not be kept in the house premises where water can accumulate as mosquitoes lays eggs in still water, and DDT must be spread in the surroundings. Researchers are carrying out to produce vaccination against malaria but till date it is not yet available. However, post malarial drugs are available in the market, as for example chloroquine and quinine.

2. Micro-cantilever and micro-cantilevered MEMS Biosensor

A rectangular beam fixed at one end and free at the other, is called a Cantilever, and a Cantilever whose dimension are in the range of microns is known as a micro Cantilever. As the dimensions of the micro Cantilever is very small, the ratios of the length to area and area to the volume will be drastically changed and these changes alter the relative effect of the various physical parameters significantly [4]. Micro-Cantilevers are one of the most advanced MEMS devices. They have been used for sensing, actuating and as a test structure. Micro-Cantilevers have potential applications as sensors in physical, chemical, biological and biomedical diagnosis [2]. They also have wide applications in the field of medicine, specifically for the screening of diseases, detection of point mutations, blood glucose monitoring and detection of chemical and biological warfare agents. These micro Cantilever-based sensors have many advantages over the conventional analytical techniques in terms of high sensitivity, low cost, simple to use, low analyte requirement, nonhazardous and quick response. Several research groups have also shown the possibility of using Micro-Cantilevers for the diagnosis of prostate cancer [2,5,6], myocardial infarction [7], and glucose monitoring [8]. Scientists are also trying to make miniaturized biochips based on array of micro Cantilevers, which will detect several routinely diagnosis diseases simultaneously in the laboratory. MEMS cantilevers are also finding applications in the radio frequency switches [9,38,40], filters [10], and resonators [11].

Cantilever based biosensors uses mechanical transduction mechanism. It is based on the bending of micro fabricated silicon cantilevers, caused by the adsorption of Bio-molecules onto the sensor surface. In biosensors applications the displacement of a cantilever can be related to the binding of Bio-molecules on the surface of the cantilever beam, and is therefore used to compute the strength of these bonds, as well as the presence of specific reagents in the solution under consideration [2,5]. Piezoresistive, piezoelectric, thermal expansion or capacitive effects are the various method for detection [4,7]. Murthy et al. (2016), presented a simple cantilever biosensor for detection of Tuberculosis by taking blood samples of affected patients. Their method for detection was based on the surface reaction of microcantilever with mycobacterium tuberculosis which results in deflection in the microcantilever but their main focus was limited to see the effect of changing beam width for deflection in designed device [12]. Saeed et al. (2016), have also presented a biosensor for detection of tuberculosis but the structure is micro stepped beam configuration which uses small portion of narrowed length and larger portion of wider length. The method of study was chosen as capacitance where the structure considers the change in the capacitance due to application of antigens. They have also done the frequency analysis for the designed structure and found that for the increased length, the device frequency decreases [13,39]. Prasad et al. (2016), presented a simulation study on a microcantilever biosensor which can detect swine flu virus. The study uses creation of stress concentrating regions (SCR) in the microcantilever for enhanced sensitivity. The use of SCRs enables a significant increase in sensitivity due to mass loading affect that is the significant stress is found in these areas of microcantilevers [14]. These microcantilever biosensors are not only limited to detect the antigens of tuberculosis, swine flu but also capable of detecting cancer biomarkers [2]. In this research, we have presented an E-shaped array of cantilever model for detection of Malaria parasites which is the cause of deadly malaria disease.

3. Stress and displacement caused in microcantilever due to biomolecules

3.1 Displacement

The micro Cantilevers often used as a mass detector that detects stripped changes of a mass attached to the surface. Many factors like Young's modulus, spring constant, Poisson's ratio, stress etc. are taken into consideration for the microcantilever that is used in the measurement. Since the thickness of the beam is very less, the moving inertia and shear deformation can be neglected. The adsorb molecules generate a surface stress on the microcantilever. This stress is created due to the interactions between the molecules and also the microcantilever surface. The relation between surface stress (σ), introduced due to analyte adsorption and deflection (d) of the beam can be expounded by Stoney's equation [15] could be a basic expression relating the residual surface stress (σ) per unit length during a film to the curvature (k) of a substrate the film is deposited onto. The curvature doesn't depend upon the fabric or the geometric properties of the film. This equation is usually employed in determinant the residual surface stresses in skinny films. In its original type, the equation was given as:

$$k = \frac{6\sigma}{Et^2} \qquad (1)$$

where E and t are the unit of modulus and also the thickness of the substrate. Since the cantilever plate is long and wide, normally follow E is replaced by the biaxate modulus $\frac{E}{(1-\vartheta)}$to accommodate the Poisson magnitude relation (ϑ) coupling. Surface stresses in solids area unit assumed analogous to the physical phenomenon in liquids. The unit of surface stress activity is totally different from that of bulk stress. For the majority stress it',s N/m^2, whereas for surfacthee stress it's ,N/m. For modelling functions the surface stress produce deflection in a substrate is commonly compared to a focused moment produce deflection in a thin plate. The pair of figures 1 shows the schematic for a cantilever plate subjected to a focused moment on its free end whereas another end is absolutely Stressful.

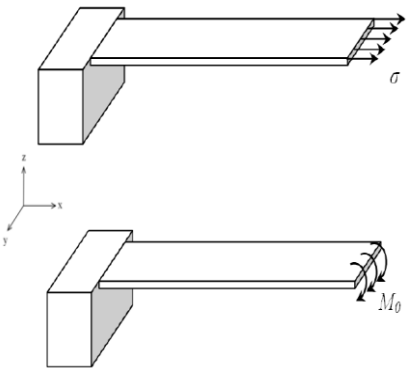

Figure 1. Simple Cantilever structure

From second figure of figure 1 the modeling surface stress including curvature during a microcantilever by equation to a targeted moment iatrogenic curvature. The targeted moment and also the surface stress are connected as $M_0 = \frac{6\sigma}{Et^2}$
where t is that the thickness of the microcantilever
Applying the Stoney equation assumption that the surface stress bends the plate with uniform curvature, into the focused moment including plate bending the subsequent curvature relation for plate bending may be given as

$$K = \frac{M_0}{EI} \qquad (2)$$

whereM_0 is the applied focused moment,
E is the modulus of elasticity of the plate,
I is the moment of inertia of the beam.
For a beam of rectangular cross-sectional, the moment of inertia is given as

$$I = \frac{bt^3}{12} \qquad (3)$$

where b is the width of the beam.
t is the thickness of the beam.
Comparing the curvature relations (1) and (2) the subsequent relation between the surface stress and therefore the moment per unit length may be established:

$$M_0 = \frac{\sigma t}{2} \qquad (4)$$

This relation shows that the moment is directly proportional to the produce surface stress and also the geometric properties of the plate. Moreover, it does not depend upon the material properties of the plate. The governing equation for associate isotropic, thin plates expressing the bending and twisting moments in terms of the curvature and also the deflection is given as [16]

$$\frac{\partial^2 z}{\partial x^2} + \frac{\partial^2 z}{\partial y^2} = \frac{M_x}{D} \qquad (5)$$

$$\frac{\partial^2 z}{\partial y^2} + \frac{\partial^2 z}{\partial x^2} = \frac{M_y}{D} \qquad (6)$$

$$\frac{\partial^2 z}{\partial_x \partial_y} = \frac{M_y}{(1-\vartheta)D} \qquad (7)$$

Where D is the flexural rigidity of the plate and $D = \frac{Et^3}{12(1-\vartheta^2)}$
In these equations, the moments are expressed in moment per unit length. Assuming $M_x = M_y = M_0$ and neglecting the shear component M_{xy}, the above equation can be written as

$$d = \frac{\sigma t(x^2 + y^2)}{4D(1+\vartheta)} \qquad (8)$$

If the cantilever is clamped in such some way that its z-direction motion is restricted, the above equation can be further simplified given as

$$d = \frac{3\sigma(1-\vartheta)}{E}\left(\frac{L}{t}\right)^2 \qquad (9)$$

Where E is the Young's modulus
$\vartheta$is the Poisson's ratio
L is the length of the microcantilever
t is the thickness of the microcantilever
Young's modulus and Poisson's ratio are material dependent, surface stress changes supported the quantity of analyte placed on the device and also the deflection of the beam varies in accordance with the changes in the length and thickness of the microcantilever beam. Deflection can be calculated for varying lengths by creating width constant and vice-versa [2]

3.2 Stress

The stress on the top of the micro Cantilever beam is $z = -\frac{t}{2}$

$$\mathrm{T(x)} = -\mathrm{E}\left(-\frac{\mathrm{t}}{2}\right)\mathrm{W''(x)} \qquad (10)$$

Now from equation

$$\mathrm{W''(x)} = \mathrm{Fx} - \mathrm{m_o} - \frac{\mathrm{Fx^2}}{\mathrm{2L}} \qquad (11)$$

and putting the value of m_o

$$W(x) = \frac{F(x^2 - 4Lx^3 + 6L^2x^2)}{24ELI} \qquad (12)$$

Now differentiating the equation 4.12 we get

$$W'(x) = \frac{F}{24ELI}\left[\frac{d}{d_x}x^4 - \frac{d}{d_x}4Lx^3 + \frac{d}{d_x}6L^2x^2\right]$$

$$W'(x) = \frac{F}{24ELI}[4x^3 - 12Lx^2 + 12L^2x]$$

$$W''(x) = \frac{F}{24ELI}\left[\frac{d}{d_x}4x^3 - \frac{d}{d_x}12Lx^2 + \frac{d}{d_x}12L^2x\right]$$

$$W''(x) = \frac{F}{24ELI}[12x^2 - 24x + 12L^2]$$

$$W''(x) = \frac{F}{12ELI}(L-x)^2 \qquad (13)$$

So,

$$T(x) = -E\left[-\frac{t}{2}\right]W''(x)$$

$$T(x) = -E\left[-\frac{t}{2}\right]\frac{F}{12ELI}(L-x)^2$$

$$T(x) = \frac{F}{4LI}(L-x)^2 \qquad (14)$$

Now putting $\mathrm{I} = \frac{bt^3}{12}$

$$T(x) = \frac{3F}{Lbt^2}(L-x)^2 \qquad (15)$$

The maximum stress at x=0 is,

$$\sigma = \frac{FtL^2}{4LI} \qquad (16)$$

Again putting $\mathrm{I} = \frac{bt^3}{12}$

$$\sigma = \frac{3FL}{bt^2} \qquad (17)$$

Where, L is the length of the microcantilever, t is the thickness of the microcantilever, b is the breadth of the microcantilever.

4. Designed structure for Biosensor

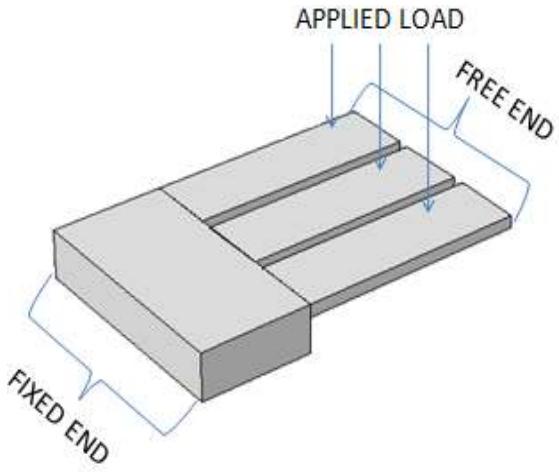

Figure 2. Proposed E-shaped array of microcantilever as sensing structure.

Design of the proposed model is shown in the Figure. 2 and steps for development of same is presented below:

Steps for Model Development

I Model environment: After opening the COMSOL Multiphysics the first job is to choose the appropriate environment for our proposed model. We choose the model wizard for selecting the space dimension. Among the 6-space dimension, we select the 3D space dimension due to our 3D model structure. Then we add our physics as solid mechanics. This interface is intended for general structure analysis of 3D, 2D, and axis symmetric bodies. After physics selection, we select our study as stationary.

II Geometry: In the model builder window we select the geometry section. In this section, the dimensions of the beam are taken depending upon the nature of the structure. First, we set the unit of the structure as a micrometer (µm). Using the build all object option in the block window we can directly make the structure as shown in figure 3.

a. First, we take the dimensions of the first block as length 5µm, breath 10µm, and thickness as 2µm.
b. Second, we take the second block to have length 10µm, breath 3µm and thickness as 0.5µm and position is set to base corner at x as10µm, y as 0µm, z as 1.5µm.
c. Third, we take the third block to have length 10µm, breath 3µm and thickness as 0.5µm and position is set to base corner at x as 5µm, y as 3.5µm, z as 1.5µm.
d. Forth we take the forth block to have length 10µm, breath 3µm, and thickness as 0.5µm and position are set to base corner at x as 5µm, y as 7µm, z as 1.5µm.

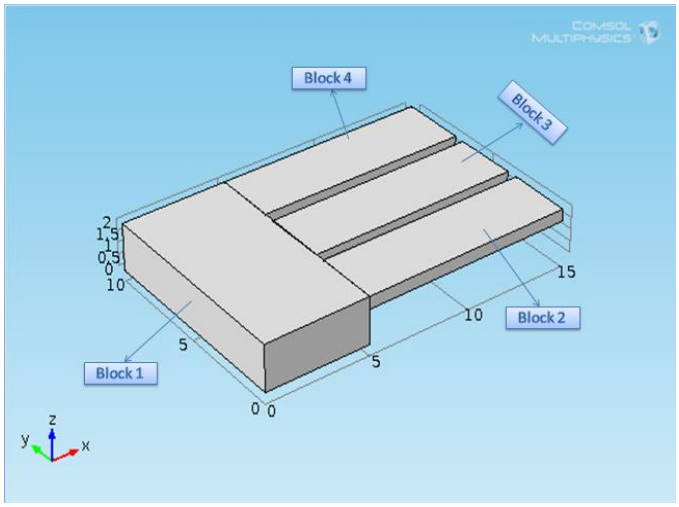

Figure 3. Geometry of the model

III Material properties: To apply the required materials to our block structure we first choose the material section in the model builder window. Then we select add material option and choose the required material from materials displayed in the right most window of the COMSOL Multiphysics. From these materials type, we first choose Ag (Silicon) and apply to the first block and then apply the Au (Gold) to the three Cantilever blocks of the structure. For the top most layers we select the solid Mechanics section and apply the Au material to it. The properties of the two materials are given in the tables .1

Table 1. Material properties

Parameters	Materials	
	Au	Ag
Young's Modulus (Pa)	70×10^9	83×10^9
Poisson's Ratio	0.44	0.37
Density (Kg/m^3)	19300	10500

IV Physics: There are various steps in the physics section that need to apply to the structure is given below.

a. Add Physics: Here for our model, we need one physics to be added. We select the add physics section in the menu bar. It enables an add physics windows at right most corner of the COMSOL main window. From which select the solid mechanics as our physics. Then we take the Solid Mechanics as our physics and it to top most layer of the structure.

b. Fixed constraint: In this section, we shall apply some boundary condition to the beam as required by the structure. We first select the physics section in the menu bar, then select the fixed constrain in the boundary option. First, we take the solid mechanics layers the left most ends of the two layers are selected and fully constrained both by displacement and rotation. So, these are the three-boundary condition at that end of the three Cantilever Beam. This makes the simple rectangular structure into an Array of Cantilever Beam.

c. Boundary load: Since the nature of the application of the beam demands uniform load. So we apply boundary load in the top surface of the Array of Cantilever Beam. We manually choose the top surface of the beam and in the load type, we select force per unit are as our load. In the first step, we vary the load from -0.1 N/m^2 to -1 N/m^2. In the second step we, fix the load as 0.5 N/m^2 throughout the simulation process. The negative sign signifies that load is in the opposite of z-axis.

V Meshing: The meshing serves two purposes. It first subdivides the structure being modeled into smaller pieces or elements over which it is possible to write a set of equations describing the solution to the governing equation. The mesh is also used to represent the solution field to the physics being solved. For meshing the structure, we first select mesh option in the menu bar and we choose the tetrahedral as our element type. Then we choose the normal meshing size to mesh the structure. Figure 4 shows the meshed model of the Array of Cantilever structure.

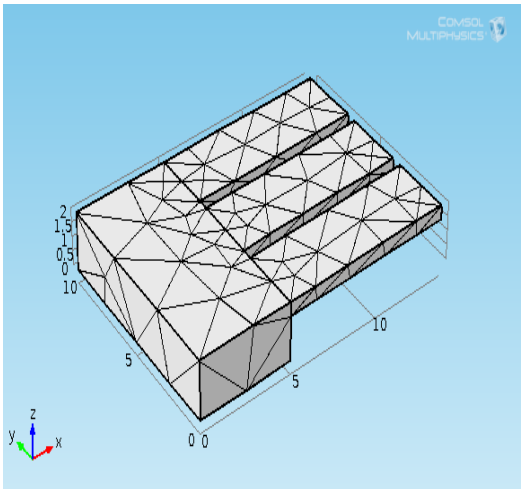

Figure 4. Meshed model of the structure

VI Study: After meshing the structure we have studied the structure for the stress and displacement are induced. In the menu bar, we go to the add study option and then compute the structure. **VII Post-processing**: The simulated result can be seen in the post-processing option of the software. We can observe that the deformed shape of the figure has different color contours. Each color contour indicates the value of the stress and deformation at different points on the beam and a scale for those colors is shown at the right. We first calculate the von-mises stress for the structure at the fixed end for the maximum stress experienced by the structure. The different stress values at the different point of the structure can be observed from the evaluation 3D window of the software at the bottom of the structure. Then we observe the deformation produced at the beam. We can see that maximum deformation is produced at the tip of the beam which is denoted by the red color contour of the structure. At last, we observe the stress and displacement produced at the upper surface of the Array of Cantilever Beam.

5. Simulation and Analytical results

The simulation process has been done with the help of COMSOL Multiphysics and the results will be analyzed in this section. Also, in order to verify the model presented for displacement and stress, we shall compare the simulated result with the analytical result. For that two steps will be considered as explained below.

Step 1:

In the first the applied load will be varied from 0.1N to 1N with a dimension of the structure remain fixed as shown in table 2 given below.

Table 2: Dimension of the model

Parameter	Block-1	Block-2	Block-3	Block-4
Length (µm)	5	10	10	10
Width (µm)	10	3	3	3
Height (µm)	2	0.5	0.5	0.5
X-Axis (µm)	0	5	5	5
Y-axis (µm)	0	0	3.5	7
Z-axis (µm)	0	1.5	1.5	1.5

In the array of Cantilever with different material, Gold has the maximum deflection followed by Silicon, Copper, and Platinum. Table 3 shows the material properties of the considered materials. Therefore, the Gold is the most suitable beam material compared to rest.

Table 3: Comparison of different material properties

Material	Young's Modulus (E)	Poisson's Ratio (υ)
Silicon	165	0.22
Gold	70×10^9	0.44
Copper	120×10^9	0.34
Platinum	168×10^9	0.38

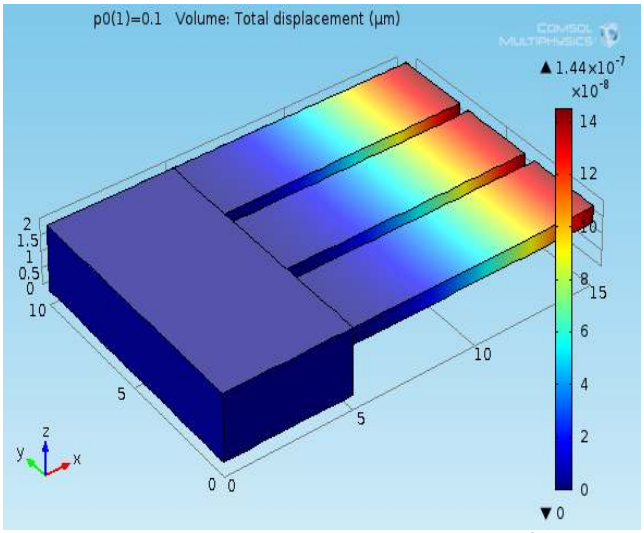

Figure 5. Displacement on the beam due to a 0.1N/m^2 load

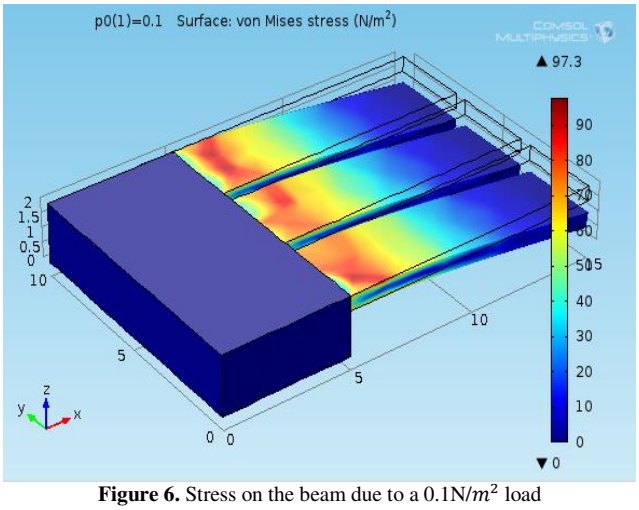

Figure 6. Stress on the beam due to a 0.1N/m^2 load

Observation Table:
The comparison of the simulated and the analytical results for stress and deflection are shown in table 4 below.

Table 4. The comparison of the analytical and simulated results for stress and deflection for varied load

S.l.No.	Load Applied	Stress(N/m^2)		Displacement (µm)	
		Analytical Results	**Simulated Results**	**Analytical Results**	**Simulated Results**
1	0.1	120	97.3	1.152E-6	1.44E-6
2	0.2	240	195	2.304E-6	2.89E-6
3	0.3	360	292	3.456E-6	4.33E-6
4	0.4	480	398	4.608E-6	5.78E-6
5	0.5	600	487	5.760E-6	7.22E-6
6	0.6	720	584	6.912E-6	8.67E-6
7	0.7	840	681	8.064E-6	1.01E-5
8	0.8	960	779	9.216E-6	1.16E-5
9	0.9	1080	876	1.0368E-5	1.30E-5
10	1	1200	973	1.1520E-5	1.44E-5

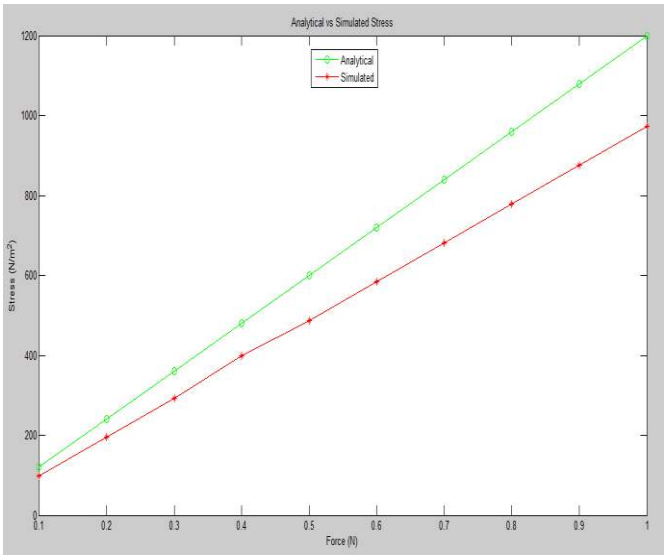

Figure 7. Comparison between analytical and simulated for Stress vs Force

Figure 6 shows the simulated stress output for an applied load of $0.1\text{N}/m^2$ .By analyzing the figure we can observe that the color contour at the fixed end of the beam is red and at the free end is blue which denote that the stress produced at fixed end of the beam is maximum and at the free end is minimum. The graph figure 7 is the comparison between the simulated results and the analytical results (from equation 17) of stress produced for different applied load. After analyzing the two curves for the analytical results and the simulated results we can observe that the both the results are almost same to each other which verify that, the model we have presented for maximum stress is accurate.

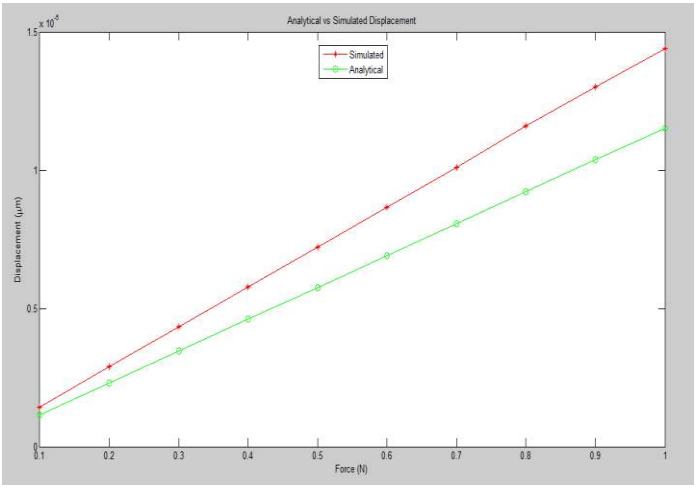

Figure 8. Comparison between analytical and simulated for Displacement vs Force

Figure 5 shows the simulated deflection output for an applied load of $0.1\text{N}/m^2$ .By analyzing the figure we can observe that the color contour at the fixed end of the beam isblue and at the free end is red which denote that the deflection produced at fixed end of the beam is minimum and at the tip is maximum. The graph figure 8 represents the comparison between the simulated deflection and the calculated deflection values. The calculated values for displacement are obtained (from the equation 9). After analyzing the two curves we see that more load is the deflection produced in the beam which can also be seen in the calculated values. After analyzing the two curves for the analytical results and the simulated results we can observe that the both the results are almost same which verify that, the model we have proposed is accurate.

Step 2:

In the first step simulated results for stress and deflection have been observed and analyzed by varying the applied load from $0.1\text{N}/m^2$to $1\text{N}/m^2$. After getting the simulated results, they are compared with the analytical results that have already been calculated using the equations mentioned. In the second case the, length of the microcantilever beam is varied from 1µm to 10µm and analyzed to see how itis affecting the resulting stress and displacement keeping other parameters constant. The applied load is kept fixed $0.5\text{N}/m^2$throughout thesimulation. As of the last case here also the simulated results are compared with the analytical results to check whether they match each other or not.

Observation Table:

The comparison of the simulated and the analytical results for stress and displacement are shown in table 5 below

Table 5. The comparison analytical and simulated results for stress and displacement for a varied length of the cantilever beam

S.l.No.	Beam length (µm)	**Stress(N/m^2)**		Displacement (µm)	
		Analytical Results	**Simulated Results**	**Analytical Results**	**Simulated Results**
1	1	6	2.95	5.75E-10	7.40E-11
2	2	24	13.1	9.216E-9	9.62E-10
3	3	54	30.6	4.665E-8	4.570E-9
4	4	96	58.6	1.474E-7	1.600E-8
5	5	150	95.1	3.600E-7	3.740E-8
6	6	216	147	7.460E-7	8.450E-8
7	7	294	223	1.382E-6	1.620E-7
8	8	384	285	2.359E-6	2.830E-7
9	9	486	388	3.779E-6	4.690E-7
10	10	600	487	5.760E-6	7.220E-7

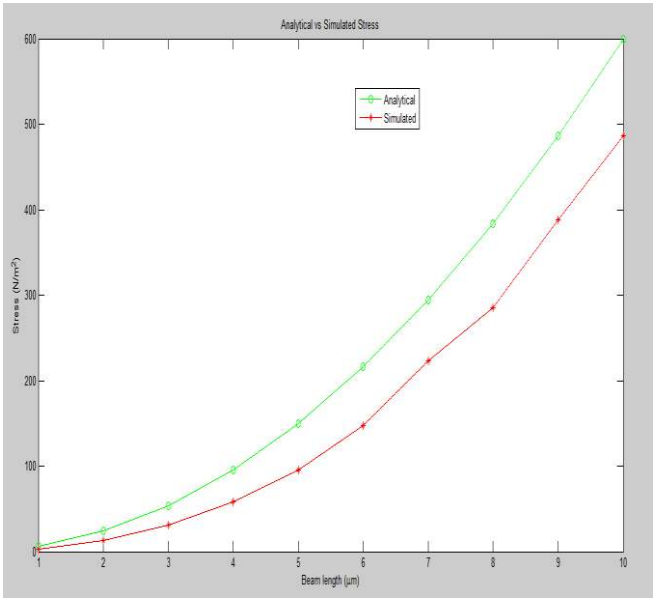

Figure 9. Comparison between analytical and simulated Stress for varied beam length

In graph fig 9 shows that the result of both the simulation and the analytical result are almost cross-pond each other and varied linearly, which prove the accuracy of the proposed model.

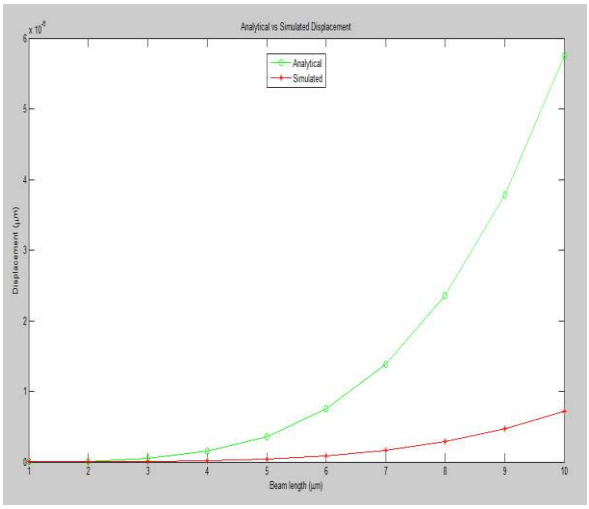

Figure 10. Comparison between analytical and simulated Displacement for varied beam length

In graph fig 10 shows that the result of both the simulation and the analytical result are almost corresponded to each other and varied linearly, which prove the accuracy of the proposed model.

Observation Table:

The simulation output result for displacement and varied beam length for different material at a fixed load 0.5 N/m^2, are shown in the table 6 below

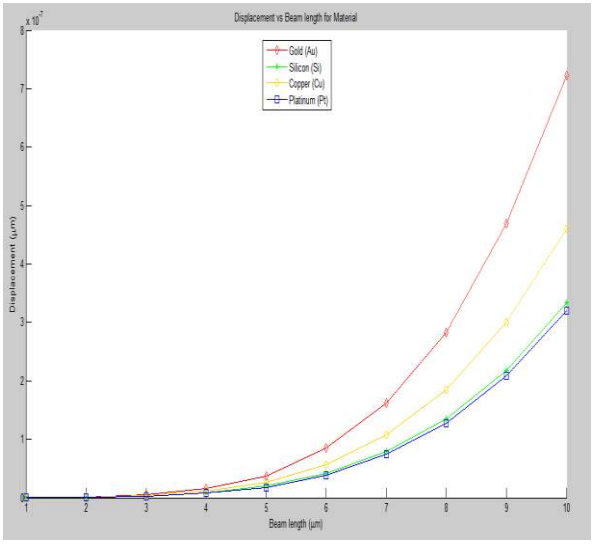

Figure 11. Simulated displacement for varied beam length for different material

In graph fig 11 shows that the simulated displacement for varied beam length for different material. The analysis of the result showed that by increase the Bio-molecules would increase the deflection and stress. Therefore, the Gold has the maximum deflection followed by Silicon, Copper, and Platinum.

6. Conclusion

A biosensor model for detection of Malaria protozoan parasites using microelectromechanical systems (MEMS) technology is presented. The presented model enables detection of protozoan parasites more accurate, easily and efficiently by using array of cantilever which is not possible to detect using traditional available biosensors. Study concludes that the deformation occurred in the microcantilever and stress developed is directly dependent on the concentration of protozoan parasites, equivalent force developed due to these parasites, length of the cantilever and most importantly selection of proper material for the microcantilever. From the selected materials viz Gold, Silicon, Copper and platinum, the best sensitivity is found to have with Gold and is mostly employed for fabrication of microcantilever based biosensors. Further studies can be performed by changing the shape of the microcantilever and use of hole in nm range over the surface of the cantilever to increase the sensitivity. Related theories for study of different vibrational elements is provided [17-37].

Acknowledgments

The authors would like to thank Department of electronics and Communication Engineering, Rajiv Gandhi University, India for providing research facility for conducting research work.

Table 6. Simulated results for displacement for varied beam length for different material

		Displacement (µm)			
Sr. No.	Beam Length (µm)	Silicon (Si)	Gold (Au)	Copper (Cu)	Platinum (Pt)
1	1	4.05E-11	7.4E-11	5.41E-11	3.63E-11
2	2	5.14E-10	9.6E-10	6.91E-10	4.67E-10
3	3	2.540E-9	4.57E-9	3.370E-9	2.260E-7
4	4	8.320E-9	1.60E-8	1.120E-8	7.590E-9
5	5	1.990E-8	3.74E-8	2.660E-8	1.800E-8
6	6	4.140E-8	8.45E-8	5.640E-8	3.880E-8
7	7	7.890E-8	1.62E-7	1.070E-7	7.400E-8
8	8	1.350E-7	2.83E-7	1.850E-7	1.280E-7
9	9	2.180E-7	4.69E-7	3.010E-7	2.090E-7
10	10	3.340E-7	7.22E-7	4.600E-7	3.200E-7

References

[1]. Rebeiz, G. M. ,2003, RF MEMS, Theory Design and Technology. Hoboken, New Jersey: Wiley.

[2]. Kurmendra, Kumar R., 2019, MEMS based cantilever biosensors for cancer detection using potential bio-markers present in VOCs: a survey, Microsyst Technol. https://doi.org/10.1007/s00542-019-04326-1

[3]. World Malaria Report (2016) , ISBN: 978 92 4 151171 1, https://www.who.int/malaria/publications/world-malaria-report-2016/report/en/

[4]. Kurmendra, Kumar R, 2017, Design analysis, modeling and simulation of novel rectangular cantilever beam for MEMS sensors and Energy harvesting applications, Int. j. inf. tecnol., 9: 295. https://doi.org/10.1007/s41870-017-0035-6

[5]. Alper Sisman, Etki Gur, Sencer Ozturk, Burak Enez, Bilal Okur, Onur Toker, 2017, A Low-cost Biomarker-based SAW-Biosensor Design for Early Detection of Prostate Cancer, Procedia Technology, Volume 27, Pages 248-249, ISSN 2212-0173, https://doi.org/10.1016/j.protcy.2017.04.106.

[6]. Keith E. Herold, Avraham Rasooly, 2012, Biosensors and Molecular Technologies for Cancer Diagnostics, CRC Press.

[7]. Vidhya S., Mathew L. ,2009, Design and Analysis of MEMS based Cantilever Sensor for the Detection of Cardiac Markers in Acute Myocardial Infarction. In: Lim C.T., Goh J.C.H. (eds) 13th International Conference on Biomedical Engineering. IFMBE Proceedings, vol 23. Springer, Berlin, Heidelberg

[8]. Y. J. Zhao, A. Davidson, J. Bain, S. Q. Li, Q. Wang and Q. Lin, 2005, A MEMS viscometric glucose monitoring device, the 13th international conference on solid state sensors, Actuators and Microsystems, Digest of technical papers, Transducers'05, Seoul, South Korea, 1816-1819, vol.2, doi: 10.1109/SENSOR.2005.1497447

[9]. Osor Pertin, Kurmendra, 2018, Pull-in-voltage and RF analysis of MEMS based high performance capacitive shunt switch, Microelectronics Journal,Volume 77, 5-15, 0026-2692 doi: https://doi.org/10.1016/j.mejo.2018.05.001

[10]. Lin F., Rais-Zadeh M., 2016, Tunable RF MEMS Filters: A Review. In: Bhushan B. (eds) Encyclopedia of Nanotechnology. Springer, Dordrecht

[11]. Abdolvand, R.; Bahreyni, B.; Lee, J.E.-Y.; Nabki, F., 2016, Micromachined Resonators: A Review. Micromachines , 7, 160.

[12]. K. S. N. Murthy, G. R. K. Prasad , N. L. N. V. Saikiran , T. V. S. Manoj, 2016, Design and Simulation of MEMS Biosensor for the Detection of Tuberculosis,ind. journ. of Sci. and techno., 9, 31.

[13]. M. A. Saeed, S. M. Khan, N. Ahmed, M. U. Khan and A. Rehman, 2016, Design and analysis of capacitance-based Bio-MEMS cantilever sensor for tuberculosis detection, International Conference on Intelligent Systems Engineering (ICISE), Islamabad, pp. 175-180. doi: 10.1109/INTELSE.2016.7475116

[14]. M.G.G. Jithendra Prasad, Syed Shameem, 2016, Design and Analysis of Micro-Cantilever Based Biosensor for Swine Flu Detection, International Journal of Electrical and Computer Engineering (IJECE), Vol. 6, No. 3, pp. 1190 ~ 1196 : 2088-8708, DOI: 10.11591/ijece.v6i3.9446

[15]. Stoney, G. G., 1909, The Tension of Metallic Films Deposited by Electrolysis, Proc. R. Soc. London, Ser. A, **82**, pp. 172–175.

[16]. https://www.doitpoms.ac.uk/tlplib/beam_bending/bend_moments.php

[17]. M Mohammadi, M Ghayour, A Farajpour, 2013, Free transverse vibration analysis of circular and annular graphene sheets with various boundary conditions using the nonlocal continuum plate model, Composites Part B: Engineering 45 (1), 32-42

[18]. M Danesh, A Farajpour, M Mohammadi, 2012, Axial vibration analysis of a tapered nanorod based on nonlocal elasticity theory and differential quadrature method, Mechanics Research Communications 39 (1), 23-27.

[19]. A Farajpour, M Mohammadi, AR Shahidi, M Mahzoon, 2011, Axisymmetric buckling of the circular graphene sheets with the nonlocal continuum plate model, Physica E: Low-dimensional Systems and Nanostructures 43 (10), 1820-1825

[20]. A Farajpour, MRH Yazdi, A Rastgoo, M Mohammadi, 2016, A higher-order nonlocal strain gradient plate model for buckling of orthotropic nanoplates in thermal environment, Acta Mechanica 227 (7), 1849-1867.

[21]. A Farajpour, MRH Yazdi, A Rastgoo, M Loghmani, M Mohammadi, 2016, Nonlocal nonlinear plate model for large amplitude vibration of magneto-electro-elastic nanoplates, Composite Structures 140, 323-336

[22]. M Mohammadi, A Farajpour, A Moradi, M Ghayour,2014, Shear buckling of orthotropic rectangular graphene sheet embedded in an elastic medium in thermal environment, Composites Part B: Engineering 56, 629-637

[23]. A Farajpour, M Danesh, M Mohammadi, 2011, Buckling analysis of variable thickness nanoplates using nonlocal continuum mechanics, Physica E: Low-dimensional Systems and Nanostructures 44 (3), 719-727

[24]. SR Asemi, A Farajpour, M Mohammadi, 2014, Nonlinear vibration analysis of piezoelectric nanoelectromechanical resonators based on nonlocal elasticity theory, Composite Structures 116, 703-712

[25]., H Moosavi, M Mohammadi, A Farajpour, SH Shahidi, 2011, Vibration analysis of nanorings using nonlocal continuum mechanics and shear deformable ring theory, Physica E: Low-dimensional Systems and Nanostructures 44 (1), 135-140

[26]. M Mohammadi, M Goodarzi, M Ghayour, A Farajpour, 2013, Influence of in-plane pre-load on the vibration frequency of circular graphene sheet via nonlocal continuum theory, Composites Part B: Engineering 51, 121-129

[27]. MR Farajpour, A Rastgoo, A Farajpour, M Mohammadi, 2016, Vibration of piezoelectric nanofilm-based electromechanical sensors via higher-order non-local strain gradient theory, Micro & Nano Letters 11 (6), 302-307

[28]. A Farajpour, A Rastgoo, M Mohammadi, 2014, Surface effects on the mechanical characteristics of microtubule networks in living cells, Mechanics Research Communications 57, 18-26

[29]. M Mohammadi, M Safarabadi, A Rastgoo, A Farajpour, 2016, Hygro-mechanical vibration analysis of a rotating viscoelastic nanobeam embedded in a visco-Pasternak elastic medium and in a nonlinear thermal environment, Acta Mechanica 227 (8), 2207-2232

[30]. M Goodarzi, M Mohammadi, A Farajpour, M Khooran, 2014, Investigation of the effect of pre-stressed on vibration frequency of rectangular nanoplate based on a visco-Pasternak foundation, JOURNAL OF SOLID MECHANICS 6 (1), 98-121

[31]. SR Asemi, M Mohammadi, A Farajpour, 2014, A study on the nonlinear stability of orthotropic single-layered graphene sheet based on nonlocal elasticity theory, Latin American Journal of Solids and Structures 11 (9), 1515-1540

[32]. M Mohammadi, A Farajpour, M Goodarzi, H Mohammadi, 2013, Temperature effect on vibration analysis of annular graphene sheet embedded on visco-Pasternak foundation, Journal of Solid Mechanics 5 (3), 305-323

[33]. M Safarabadi, M Mohammadi, A Farajpour, M Goodarzi, 2015, Effect of surface energy on the vibration analysis of rotating nanobeam, Journal of Solid Mechanics 7 (3), 299-311

[34]. M Goodarzi, M Mohammadi, M Khooran, F Saadi,2016, Thermo-mechanical vibration analysis of FG circular and annular nanoplate based on the visco-pasternak foundation, Journal of Solid Mechanics Vol 8 (4), 788-805

[35]. M Mohammadi, M Ghayour, A Farajpour, 2011, Analysis of free vibration sector plate based on elastic medium by using new version differential quadrature method, Journal of solid mechanics in engineering 3 (2), 47-56

[36]. M Mohammadi,A. Rastgoo, 2018, Primary and secondary resonance analysis of FG/lipid nanoplate with considering porosity distribution based on a nonlinear elastic medium , Mechanics of Advanced Materials and Structures, DOI: 10.1080/15376494.2018.1525453

[37]. M. Mohammadi and A. Rastgoo, 2019, Nonlinear vibration analysis of the viscoelastic composite nanoplate with three directionally imperfect porous FG core, structural engineering and mechanics, pages 131-143. DOI: 10.12989/sem.2019.69.2.131

[38]. Kurmendra, R. Kumar, 2019, Design and Simulation of MEMS shunt capacitive switch for lower switching time, Special Issue (2019): 3C TECHNOLOGY - EDITION 28-2. DOI: 10.17993/3ctecno.2019.specialissue.15

[39]. Kurmendra, Kumar R., Pertin O. , 2019, Design of An Improved Micro-Electro-Mechanical-Systems Switch for RF Communication System. In: Khare A., Tiwary U., Sethi I., Singh N. (eds) Recent Trends in Communication, Computing, and Electronics. Lecture Notes in Electrical Engineering, vol 524. Springer, Singapore DOI: https://doi.org/10.1007/978-981-13-2685-1_1

[40]. A. Chamuah, Kurmendra and R. Kumar, 2018, A Novel Structure for Piezoelectric Based MEMS Energy Harvester, 5th IEEE Uttar Pradesh Section International Conference on Electrical, Electronics and Computer Engineering (UPCON), Gorakhpur, 2018, pp. 1-4. doi: 10.1109/UPCON.2018.8596823